Electronic Supplementary Material (ESI) for Lab on a Chip.

Electronic Supplementary Information (ESI) for

Microfluidic valvular chip and numerical lymphatic vessel model for study of lymph transport characteristics

Jaemin In, Jihye Ryu, Hyeonji Yu, Dongwon Kang, Taeyoung Kim, and Jungwook Kim*

Department of Chemical and Biomolecular Engineering, Sogang University, Seoul, South Korea.

Correspondence to: jungwkim@sogang.ac.kr

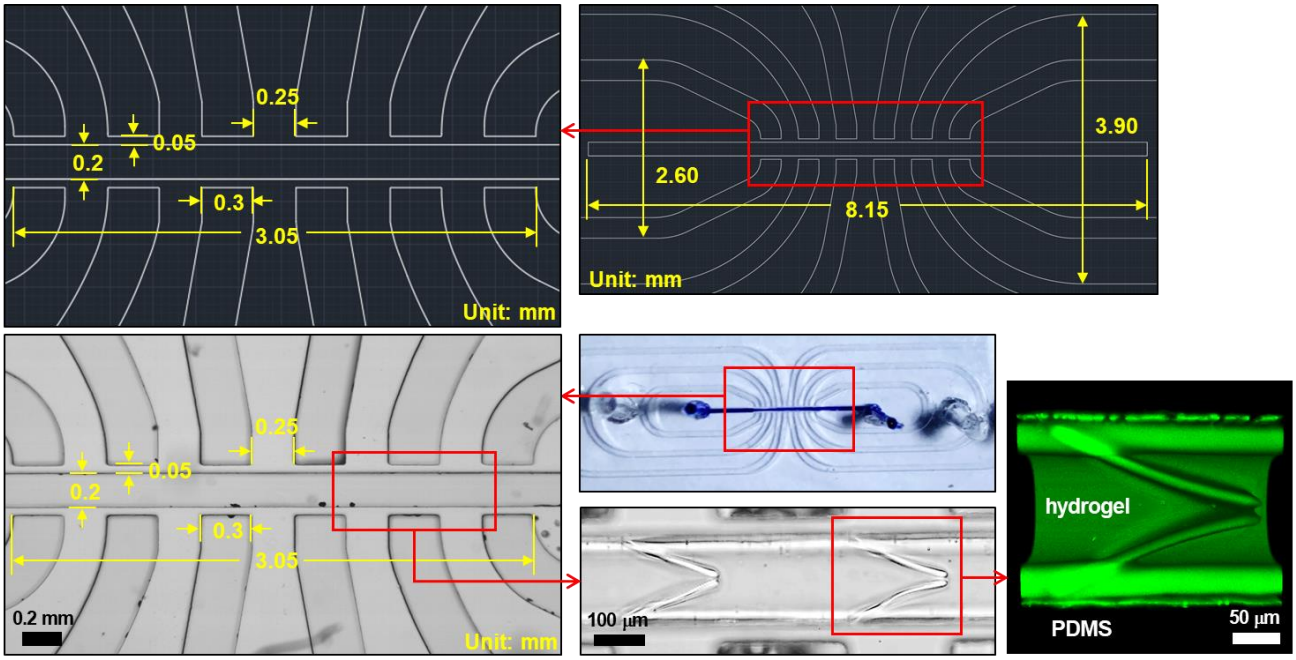

Figure S1. Details of the geometry and dimensions of the PDMS microfluidic device and hydrogel luminal structure with the bicuspid valve leaflets. Top images correspond to the CAD design.

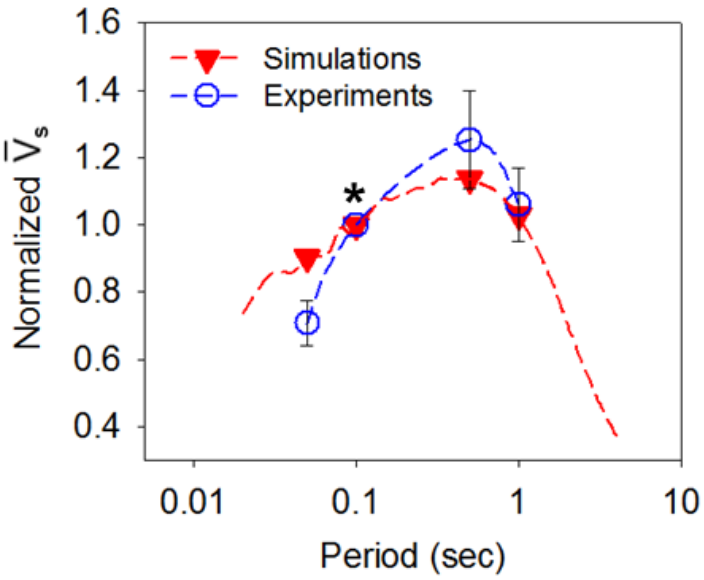

Figure S2. The simulation results for the dependency of $\bar{V}_s$ on the compression period was reproduced experimentally using the microfluidic valvular chip. An asterisk indicates the data points used for normalization of experimental and numerical results.

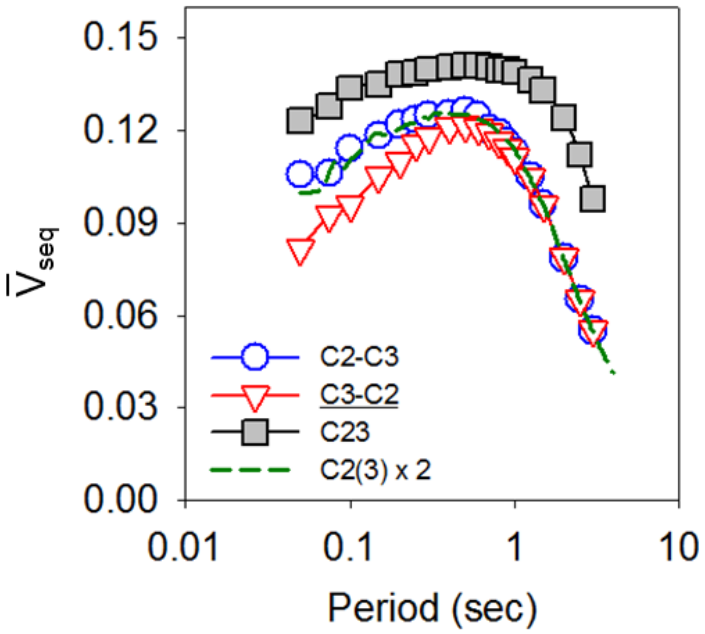

Figure S3. The dependency of $\bar{V}_{seq}$ on the compression period for varying sequences. The optimum periods corresponding to the maximum $\bar{V}_{seq}$ are 0.6, 0.5, 0.4, and 0.5 s for C23, C2-C3, C2(3), and C3-C2, respectively. The phase delay is 1.0, and the contraction fraction is 6 %.

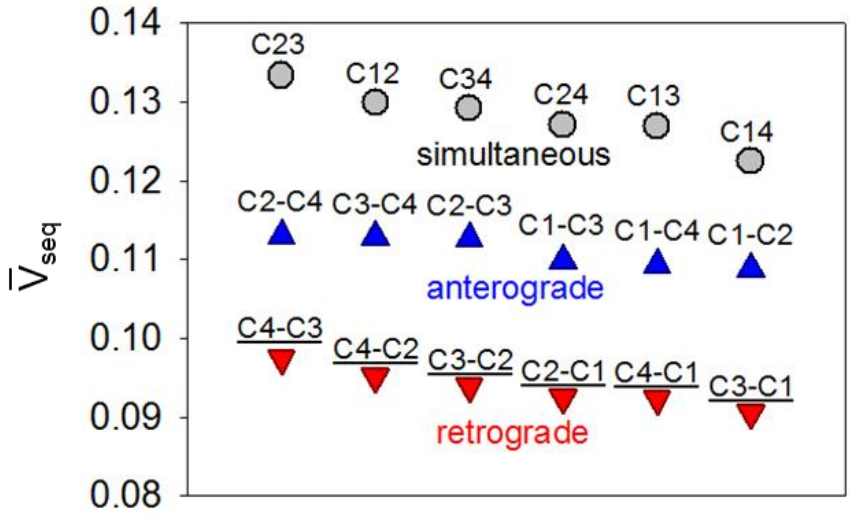

Figure S4. $\bar{V}_{seq}$ calculated for various sequences of compressing two chambers, which are indicated above each data point. The contraction fraction is 6 %, and the period is 0.1 sec. The phase delay for the anterograde and retrograde sequences is 1.0.

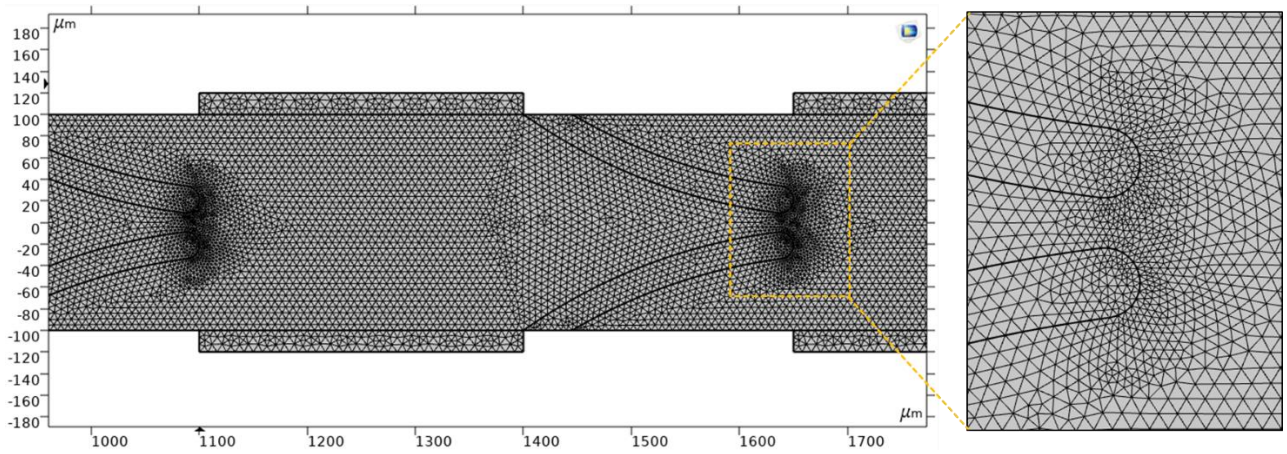

Figure S5. The numerical lymphatic vessel model constructed in the Fluid-Structure Interaction interface using COMSOL. 56,498 elements were used to mesh the model, where the fluid mesh was refined in regions between the valve leaflets (right).

Table S1. Comparisons in geometry and mechanical properties between the rat mesenteric lymphatic vessel and our systems.

		Rat mesenteric lymphatic vessel	Our systems		Ref.
			Microfluidic chip	Numerical model	
Geometry	$L_{v\text{-}to\text{-}v}$	400-500 μm	550 μm	550 μm	6
	L_v	120-140 μm	210 μm	250 μm	6
	D	100-300 μm	125 μm	200 μm	6
	d_0	2 μm*	5-10 μm	20 μm	6
Valve leaflet	Young's modulus	58 kPa#	40 kPa	Soft: 40 kPa Rigid: 4 MPa	11
	Poisson's ratio	0.45*	Not measured	0.49	11
Lymph	Viscosity	1.08-1.36 mPa·sec	1/3-3 mPa·sec	0.89 mPa·sec (water)	2
	Density	1.005-1.016 g/ml	1.00 g/ml (water)	1.00 g/ml (water)	2
Active pumping	Contraction fraction	5-50 %	0-20 %	0-22%	18
	Period	~0.5-3 sec	0.05-1 sec	0.01-5 sec	19-21
	Phase delay	0-0.5*	0-2	0-3	3, 8
	Sequence	Antero- and retro-grade, simultaneous	Antero- and retro-grade, simultaneous	Antero- and retro-grade, simultaneous	3
	Pressure difference	±20 mmH_2O*	Not applied	±8 mmH_2O	7

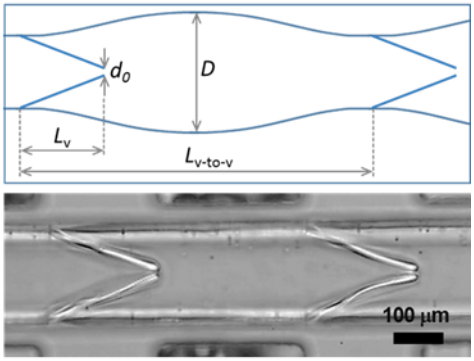

* These are values used in the existing analytical or numerical studies based on the in vivo or ex vivo measurements.

Shear modulus of 20 kPa was converted to Young's modulus assuming isotropic and homogeneous materials with Poisson's ratio of 0.45.

Table S2. Sequences of compression of four adjacent chambers classified based on Ns and Nr. Number in parentheses indicates total number of sequences in each classification.

N_r \ N_s	1	2	3	4
0	(1) 1-2-3-4	(3) 12-3-4 1-23-4 1-2-34	(2) 1-234 123-4	(1) 1234
1	(11) 1-2-4-3 1-3-2-4 1-3-4-2 1-4-2-3 2-1-3-4 2-3-1-4 2-3-4-1 2-4-1-3 3-1-2-4 3-4-1-2 4-1-2-3	(22) 12-4-3 1-24-3 13-2-4 1-3-24 13-4-2 1-34-2 14-2-3 1-4-23 2-13-4 2-1-34 23-1-4 2-3-14 23-4-1 2-34-1 24-1-3 2-4-13 3-12-4 3-1-24 34-1-2 3-4-12 4-12-3 4-1-23	(6) 124-3 134-2 2-134 234-1 3-124 4-123	Not available
2	(11) 1-4-3-2 2-1-4-3 2-4-3-1 3-1-4-2 3-2-1-4 3-2-4-1 3-4-2-1 4-1-3-2 4-2-1-3 4-2-3-1 4-3-1-2	(11) 14-3-2 2-14-3 24-3-1 3-14-2 3-2-14 3-24-1 34-2-1 4-13-2 4-2-13 4-23-1 4-3-12	Not available	Not available
3	(1) 4-3-2-1	Not available	Not available	Not available